International Journal of Computational and Experimental Science and ENgineering (IJCESEN)

Vol. 12-No.2 (2026) pp. 169-178
http://www.ijcesen.com

ISSN: 2149-9144

Research Article

Vibrational Properties at the Intersection of Embedded Nanostructure and Surface Boundary

Belabbaci Mohammed[1], Bouchareb. Sansabilla[2]*, LASRI Boumediène[3], Tigrine Rachid[4,5]

[1]Laboratoire de Physique Théorique (LPT) ,Université Ahmed Draya Adrar Algérie
Email: belabbac2i@gmail.com- **ORCID:** 0000-0002-5247-7833

[2]Laboratoire d'énergie, environnement et systèmes d'informations Université Ahmed Draya Adrar Algérie
* **Corresponding Author Email:** sansabilla123@gmail.com - **ORCID:** 0000-0002-5247-7877

[3]Laboratoire de Physique Théorique (LPT) , Université Abou-Bekr Belkaïd, Faculté des Sciences, Département de Physique, B.P 119, Tlemcen (13000), Algérie.
Email: lasr2i@gmail.com- **ORCID:** 0000-0002-5247-4325

[4]Laboratoire d'énergie, environnement et systèmes d'informations Université Ahmed Draya Adrar Algérie
[5]Laboratoire de Physique et Chimie Quantique, University Mouloud Mammeri de Tizi-Ouzou, Algeria.
Email: tigrin2e@gmail.com- **ORCID:** 0000-0002-5247-6723

Article Info:

DOI: 10.22399/ijcesen.5136
Received : 15 March 2025
Revised : 03 February 2026
Accepted : 11 April 2026

Keywords

surface and interface;
nanostructures;
defects;
electronic scattering;
localized phonons;
matching method

Abstract:

We propose an analytical approach to investigate the vibrational scattering and localization at the intersection of an embedded nanostructure and boundaries of crystalline surfaces . The propagating and the evanescent modes are calculated in the bulk material and the energies of localized modes in the neighbourhood of the defect are determined. We show respectively the existence of optical localized modes and acoustical modes induced by the inhomogeneity. Also the number and features of these curves depend strongly of the parameters of a system model. The state densities are calculated by the mean of the Green functions associated to the matching method, for atomic sites that constitute a minimum representation set in the neighbourhood of the defect. The interaction between the propagating bulk modes and the localized phonons induced by the integrated nanostructure give rise to resonances in the subband of the bulk material

1. Introduction

It has been found that a large variety of products possess intrinsic vibrational characteristics that provide a signature of their state. Sometimes these characteristics are chemical, optical, electrical, magnetic or mechanical in nature. Regardless, there is much commonality in the basic measurement and analysis process applied in assessing the state of product. The key feature of the dynamic process is the integration of fast, continuous response measurement devices, high-speed data acquisition, advanced time and frequency domain signal processing, data analysis and production line disposition and control. Further, integration on the analysis side should merge statistical analysis methods with techniques of time and frequency domain finger printing. The present article will focus on the use the elecronic characteristics for rating product state. However, various methods can be applied to measured parameters associated with other kinds of product characteristics. Furthermore, the identification of structural defects in mechanical products is an important task in industrial production and checking worm, but still valuable component. In the field of non destructive control different methods have been developed for this purpose. There are the powerful engineering methods for investigating the vibrational properties and vibration behaviour of mechanical objects by laser scanning.

The study of scattering and localization phenomena in disordered systems have been interest for a long time,[1,2] because of their use as components in high technology devices. A direct observation of the electronic dispersion relation of lattice is not possible because sound waves of sufficiently high frequencies are not available. Also, there are two

techniques that are often used to experimental study phenomena, and in particular to measure elect dispersion relations on ordered surface, such as : the angular resolved electron energy loss spectroscopy (EELS) [3,4] and helium atom scattering (HAS) at thermal energies.[5] In comparison with experimental work, the dispersion relation on ordered surface are determined usually in the harmonic approximation,[6,7] using several suitable methods then Green functions [8] the slab [9,] and the matching methods [10-12.] The physical properties are influenced by the structure and the nature of defect. Even well polished, the surface lattice presents the inhomogeneity. This can be confirmed from experimental exploration techniques using the tunnel effect, such as the Scanning Tunnelling Microscopy (S.T.M) or the Columbian interaction, such as the Atomic Force Microscopy (A.F.M), with the possibility to access to a direct evaluation of the surface state. Many theoretical studies have been made on this subject [13-21,] but no work has been done about the vibrational properties of defect planar in crystallographic simple cubic system. In this practical case, the perfectly periodic disposition does not exist and this implies that the disorder must be considered.

The full study of a system with surface disorder is still a difficult exercise. Our study uses the harmonic approximation, and the equation must consider central interactions between nearest and next nearest neighbours, in order to respect the atomic stability condition.

Since the temperature is not zero, the lattice is not at equilibrium, and the atoms oscillate with amplitude and energy depending on the solid temperature. Concerning the study of surface vibrational modes at the intersection of an embedded planar defect with the surface boundary, the absence of translational symmetry in the direction perpendicular to the defect and to the surface, prohibits the use of the Bloch theorem along these directions.

It is here necessary to use an appropriate method which limits the number of equations; for example the matching method. In section 2 a complete description of the model is given and in the section 3 the dynamical properties are presented for the bulk. The theoretical formalism for calculating the localized phonons is described in section 4 and in section 5 the spectral and state densities are given. Section 6 gives the principal numerical results and their interpretations and the general conclusions of the paper.

2. Description of the model

The model for the class of extended boundary defect system and it projection in the plane XOY are presented respectively in Fig.1.a and Fig.1.b a. It consist of an isolated planar of Cu atoms integrated in cubic crystal of atoms of polonium (Po). The system is indexed by n, s and l. The presence of the discontinuity and the surface produce a breaking of the translational symmetry in two directions. The defect and its environment differ from the rest of the system by their elastic properties and by masses different of Cu and Po atoms. Further the quantities $k_1(i,j), k_1^{'}(i,j), k_1^{''}(i,j), k_2(i,j)$ and $k_2^{'}(i,j)$ stand respectively nearest and next nearest strength constants for Po-Po, Cu-Po, Po-Po interactions.
The parameters r_0, r_1, r_2, r_3, r_4 and e' are given as

$$r_0 = \frac{k_2(Po-Po)}{k_1(Po-po)}, r_1 = \frac{k_1^{'}(Cu-Po)}{k_1(Po-Po)},$$
$$r_2 = \frac{k_2^{'}(Cu-Po)}{k_1(Po-Po)}, r_3 = \frac{k_1^{''}(Cu-Cu)}{k_1(Po-Po)},$$
$$r_4 = \frac{k_2^{''}(Cu-Cu)}{k_1(Po-Po)}, \; e^{'} = \frac{M_{Cu}}{M_{Po}}.$$

They are respectively the ratios of the *next nearest neighbour* (*nnn*) force constants k_2(*Po-Po*), the *nearest neighbour* (*nn*) k'_1(*Cu-Po*), (*nnn*) k'_2(*Cu-Po*), and the (*nn*) k''_1(*Cu-Cu*) and (*nnn*) k''_2(*Cu-Cu*), with respect to the (*nn*) k_1(*Po-Po*) force constant.

3. Vibrational dynamics on the perfect waveguide.

We describe the evanescent vibrational field of a simple cubic crystal bulk, sufficiently removed to the right and the left far from the defect plane, by the phase factors (η_2, η_2^{-1})going from one site to its nearest neighbours, respectively along the axes parallel and normal to the system boundary, Fig.2. The following relations may then define these factors:

$$u(n',s'') = u(n,s)\eta_2^{n'-n}e^{i(s'-s)}$$
$$v(n',s'') = v(n,s)\eta_2^{n'-n}e^{i(s'-s)} \qquad (1)$$

Where u, v denote the Cartesian components of the vibration displacements for a given sites, respectively in the x and y direction. Consider an elementary domain $\coprod_v$, containing a bulk Po sites and its nearest and next nearest neighbours, sufficiently removed both far from the defect and from the boundary. The necessity of introducing the relations of Eq.1 is inherent to the matching

method. The bulk secular is hence obtained from the motion equation [22] and Eq.1

$$A_3\,\eta_2^3 + A_2\eta_2^2 + A_1\,\eta_2 + A_0 \qquad (2)$$

The non degenerate solutions η_{2i} of Eq .3 as function of the vibrational frequency, of the elastic constants and the atomic masses of defect and the host lattice, determine the accessible evanescent modes in the direction parallel to the boundary (x) For the case of a simple cubic lattice these solutions correspond to twelve roots of Eq.3 .However, only four these solutions satisfying the condition $|\eta_{2i}|<1$ can be retained to describe the evanescence. For the ensemble of evanescent solutions $\eta_{2,i}$, Eq.3 gives in turn the set of non degenerate evanescent modes $\eta_{2,i}$ that determine the evanescent modes in the direction normal to the boundary. In all we have $[\eta_2(i)],i\in[1,4]$ The all phase factor, represented on the Fig.1 verify the hermitical nature in bulk dynamics equivalent to time reversal symmetry in crystalline lattices [23].

This completes the description of the evanescent field vibrations in the bulk of the simple cubic lattice and permits the construction of a basis over the evanescent modes.

4. Localized states at the boundary defect

The dynamics of the planar defect at the boundary is described by the equation of motion over domain Π_2, defined by $n\in[-5,5]$, s=1 , $l=0$, that contains the intersection of isolated planar defect with cubic surface. The choice of the site Π_d should preserve the intrinsic symmetry and must contain a sufficient number of atoms for completeness. The equations of motion over this domain can be projected onto distinct domains Π_1 and Π_2, which delimit the boundary defect as a molecular object, or an irreducible set of atoms at the defect necessary to describe the system, represented by the site, **a(-2,1,0)**, **b(-1,1,0)**, **c(0,1,0)**, **d(1,1,0)** and **e(2,1,0)**. The other sites in Π_d can be folded onto sites in Π_2, indicated in Fig.1b, which domain represents the matching region of the system. The displacements of surface atoms (l =-1) are expressed as function of bulk atom displacements by matrix inversion [24]. The second objective is to express the displacements of domain Π_2 in the Hilbert space basis of the evanescent modes of the bulk domain. Let $\{R_{i,j}\}$ denote a set of basis vectors for the evanescent modes in the domain Π_2. The number of these vectors for the cubic simple lattice with nearest and next nearest interactions is given by Eq.3.

This basis is defined for the directions perpendicular to the defect boundary by two unitary vectors: $\{R_{21}^{-1},R_{22}^{-1},\}$ and $\{R_{21}^{+1},R_{22}^{+1}\}$ for the left and right quarter-infinite Po bulk spaces respectively. The distinction between right and left is useful in order to set up from the beginning a framework not only for study of localized phonons but also for the analysis the scattering phenomena of the isolated planar. In this work we present the localized phonons and scattering elastic wave are presented and discussed. Each site in the domain Π_1 can be expressed in the basis $\{R_{i,j}\}$ [25]

For ($m\le -3$, $l=0$):

$$u(n,s)=\sum_{j=1}^{n2}R_{2,j}^{-1}A(u,\eta_{2,j})\eta_{2,j}^{n_s-n}$$

$$v(n,s)=\sum_{j=1}^{n2}R_{2,j}^{-1}A(v,\eta_{2,j})\eta_{2,j}^{n_s-n} \qquad (3a)$$

For($m\ge 3, l=0$):

$$u(n,s)=\sum_{j=1}^{n2}R_{2,j}^{+1}A(u,\eta_{2,j})\eta_{2,j}^{n_s-n} \qquad (3b)$$

$$v(n,s)=\sum_{j=1}^{n2}R_{2,j}^{+1}A(v,\eta_{2,j})\eta_{2,j}^{n_s-n}$$

Where (n_s, s_s) represent the coordinates of the reference sites; in our model is, we choose (0, 0, 0) site, n_2 represent the numbers of associated evanescent modes. $A(u,\eta_{2,i})$ and $A(v,\eta_{2,i})$ denote relative weighting factors associated with and u and v displacement amplitudes. Using Eq.3 we define a matching matrix denote M_r, that folds the vibration displacements on the bulk sites onto the basis $\{R_{i,j}\}$. The irreducible sites are unaffected by this transform. The product of the dynamics matrix in the perturbed region M_d with the matching matrix M_r, yields a square matrix M_s and linear inhomogeneous system of equations:

$$\left[\Omega^2 \mathrm{I}-M_s(\phi_z,r_0,r_1,r_2,r_3,r_4,\eta_2(j)),\left\|U_r\right\rangle,\left|R_{2,i}^{-1}\right\rangle,\left|R_{2,i}^{+1}\right\rangle\right]=|0\rangle \qquad (4)$$

The Ω is the dimensionless frequency given by $\Omega^2=\dfrac{\omega^2}{\omega_0^2}$ ω_0 is a characteristic lattice frequency given by $\left(\dfrac{k_1(P_0-P_0)}{M_{P_0}}\right)^{1/2}$, and $\phi_z=aq_z$, being the one-dimensional reciprocal lattice wave vector along the z . A non trivial solution of Eq.4 yields the

energies of localized modes, represented on a Fig.2, as a function of the system parameters: for respectively $r_0 = 0.25$, e'= 0.3, r1=0.76, r2 = 0.12, $r_3 = 0.63$, $r_4 = 0.063$ and φ_z running over [0, 3.5] the other parameters remaining fixed. In the Fig.2, the modes outside the phonon band limits represent the dispersion curves of the localized phonons on the defect plan and surface boundary They illustrate the presence of the surface and the breakdown of the translational symmetry due to the presence of a planar defect. Several localized phonon modes appear which are inexistent in the bulk material. The Einstein modes of the high frequencies are situated below the bulk sub band. The other resonant modes are in the interval frequencies Ω = 0.5-3.5, which represent the limit bulk band of the system. The acoustical modes are under the bulk band vibrations.

5. State densities at the perturbed domain

For completeness the calculated DOS for sites in the bulk and in the unreconstructed (001) Polonium surface and planar defect, are presented. The Green functions being are useful to calculate the spectral and state densities and the matching method gives a very compact formulation of these functions [26] :

$$G(\phi_z, \Omega^2 + i\varepsilon) = \left[(\Omega^2 + i\varepsilon)I - M_S(\phi_z, r_0, r_1, r_2, r_3, \lambda, \{\eta_2\})\right]^{-1} \quad (5)$$

The Green operator is then obtained from the square matrix M_S. The spectral density matrix, for a given wave vector parallel to the line defect, is then given by the following equation:

$$\rho^{(l,l')}_{(\alpha,\beta)}(\phi_z, \Omega) = 2\Omega \sum_m p^l_{\alpha m} p^{l'}_{\beta m} \delta(\Omega^2 - \Omega^2_m) \quad (6)$$

Where l and l' represent two different atoms, α, β are two different Cartesian directions, and $p_{\alpha m}$ is the α component of the polarisation vector on the atom at l for the mode of frequency Ω_m. The density of states is obtained by a sum on ϕ_z of the trace of the spectral density matrix:

$$D(\Omega) = \sum_{\phi_z} \sum_{l\alpha} \rho^{(l,l)}_{(\alpha,\alpha)}(\phi_z, \Omega) = -\frac{2\Omega}{\pi} \sum_{\phi_z} \sum_{l\alpha} \lim_{\varepsilon \to 0^+} \left\{ \mathrm{Im}\left[G^{ll}_{\alpha\alpha}(\phi_z, \Omega^2 + i\varepsilon) \right] \right\}. \quad (7)$$

The dashed (dotted) spectra in Figs.3: (a) and (b) correspond to the localized DOS for bulk and surface sites, respectively (**a**), (**b**). Their evolutions are represented as a function of the parameters of the system: respectively for $r_0 = 0.25$, e'= 0.3, r1=0.76, $r_2 = 0.12$, $r_3 = 0.63$, $r_4 = 0.063$ and dimensionless frequencies Ω. The vibrational state densities, present several resonance peaks in the range of Ω between 0 and 3.5. This range corresponds to frequency of the limit phonon bulk band. One observes for all the spectral densities , two types of the peaks, those on the one hand with big amplitudes corresponding to resonant modes of the bulk or to localized phonons over a Brillouin zone and on the other those with weak amplitude corresponding to the localized phonons situated below a Brillouin zone. We note that the width, the height and the number of peak resonances depend strongly on structural parameters of the system.

6- Elastic wave scattering by the defect

For an incoming propagating wave corresponding to the eigenmode i at a frequency Ω and incident from the left to right, the resulting scattered waves at Ω, are composed of a reflected and a transmitted part. The Cartesian components α of the displacement field U(n,n') for an outside atom bordering the defect domain [-1, 1], may be expressed using the matching approach. For a site inside the wave guide to the left of the defect, the displacement field $U_\alpha(n,n')$ can be expressed as the sum of the incident wave and a superposition of the eigenmodes of the bulk reflected by the scatter at the same frequency.

$$U_\alpha(n,n') = u_i \eta_i^n + \Sigma_j \eta_j^{-n} R_{ij} u_j \quad \text{with} \quad n<-3 \quad (8)$$

where the vectors u_i and ηdenote respectively the eigenvectors and the eigenvalue of the dynamic matrix for the perfect wave-guide at the frequency Ω. R_{ij} are the reflection coefficients that describe the scattering of a given incident wave i into the eigenmodes j =1. For a site inside the wave guide to the right of the defect, the displacement field $U_\alpha^+(n, n')$ can be expressed by an appropriate superposition of the eigenmodes of the perfect wave guide transmitted by the defect at the same frequency

$$U_\alpha^+(n,n') = \Sigma_j \eta_j^n T_{ij} u_j \text{ with } n>3 \quad (9)$$

T_{ij} are the transmission coefficients for incident wave i into the eigenmodes j =1.

Consider a Hilbert space for the scattering and denote by [|R>, |T>] the basis vector for the reflection and transmission coefficients in this space, and by |U>that for the displacements of a set of irreducible sites in the defect domain. The equations of motion for the defect, coupled to the rest of the systems, may be written in terms of

vector [|U>, |R>, |T>]. Using the transformations connecting the displacement fields in Eqs (4)-(5), we obtain a square linear inhomogeneous system of the equations of the form

$$[\Omega^2 I - D(\eta, r)]\ [|U>, |R>, |T>] = -|IH> \qquad (10)$$

Where the vector -|IH>, mapped appropriately onto the basis vectors, regroups the inhomogeneous terms describing the incoming wave.

The solution of Eq(10) yields the displacements |U> of the irreducible set of atomic sites for the defect domain [-2, 2], as well as the reflection and transmission coefficients R_{ij} and T_{ij} on the perfect wave-guides.The scattering behaviour is usually described in terms of the scattering matrix, which elements are given by the relative reflection and transmission probabilities r_{ij} and t_{ij} at the scattering frequency Ω. These are given by

$$r_{ij} = (V_{gi} / V_{gi}) \left| R_{ij} \right|^2 \text{ and } t_{ij} = (V_{gj} / V_{gi}) \left| T_{ij} \right|^2 \qquad (11)$$

Where in order to obtain unitarity of the scattering matrix, the scattered elastic waves have to be normalised with respect to their group velocity. V_{gs} is the group velocity of the eigenmodes, put equal to zero for evanescent modes [28-41]. Typical results for the group velocities of the three eigenmodes are presented in Fig.3 for r = 0.25.Some modes show regions of anomalous dispersion where the group velocity is negative: these regions require a careful examination of the notion of forward and backward scattering for the waves.We can further define total reflection and transmission probabilities for a given eigenmode at scattering frequency Ω by summing over all the contributions

$$r_i(\Omega) = \sum_j r_{ij}(\Omega) \text{ and } t_i(\Omega) = \sum_j t_{ij}(\Omega). \qquad (12)$$

Furthermore, in order to describe the over all transmission of mesoscopic multichannel systems at a given frequency Ω, it is useful to define the conductance of the system (or the domain defect transmittance) t(Ω), by summing over all input and out put channels

$$t(\Omega) = \sum_i \sum_j t_{ij}(\Omega) \qquad (13)$$

Where the sum is carried out over all propagating modes at frequency Ω. The transmission probabilities $t_i(\Omega)$ per eigenmode i, and the conductance of the system t(Ω), are important to calculate because each corresponds indeed to an experimentally measurable observable.

7. Numerical results and general conclusions

We establish, rigorously, a complete cartography of the vibrational field around the surface crystalline and the defect plan using the matching method. The specific advantage of our matching method, compared to other methods such as the cluster numerical approach, and besides being transparent at all stages of the calculation, is that it gives an exact and rigorous analytical formulation of the vibrational field displacements in the limit to infinity. There are no numerical approximations. The Rayleigh modes parallel to the Oz axis which represent high symmetry of the system are hence calculated in an efficient computational scheme. The dynamical properties at the line defect and its neighbourhood gives different types of vibration modes. Their number is large, however, they separate naturally into three types, type one consists of the surface phonons corresponding to region far from the defect, which are reflected and transmitted by the defect. The second class, no existent in perfect wave guide, consists of the localized phonons which are vanishes in part and other one of the inhomogeneity, the third class is Rayleigh phonons propagate freely, in the direction parallel to the defect, direction of the high symmetry of the system. One shows that a defect is a generator of localized phonons in the system and the variation of the system parameters affects considerably the different properties of the lattice then the vibrational and thermal properties. The interaction between the localized phonons and the vibrational modes of the bulk gives the resonances peaks [27- 29.] It's possible to exploit the physics properties of disordered system to build the filter and the probe frequencies which are used in not destroyed control. We are able to use the localisation and scattering properties for investigation and characterizing the nature of structure various defects. The elastic waves of Rayleigh are a best know example of macroscopic phonons. At the large wave-lengths, they are no dispersive and their properties are well described by the continuum theory; Long-wavelength Rayleigh modes find extensive application in the high technology as the electroacoustical microelectronic device because of their small damping, constant velocity and the accessibility, provided to by to their surface localization. The dispersion relation of surface phonons is important for understanding the physics of solid surface [30-34.] surface phonons, also play an important role in gas–surface interactions [35-37].The energy transfer from atoms and molecules to phonons is fundamental to understanding of accommodation coefficients and adsorption and desorption kinetics, as well as sticking coefficients. These are all importance elementary steps in catalysis. It is hoped that this calculation will

generate interest for experimental measurements of the bulk and surface phonons of this material.

Numerical calculations are presented for three cases of a lamellar sfc Cu nanostructure between bcc Po leads, of the-Po[Ni(*n*)]Fe-system, where n = 1,3, the system parameters: for respectively r_0 = 0.25, e'= 0.3, r1=0.76, r2 = 0.12, r_3 = 0.63, r_4 = 0.063 .

The dispersion curve $\Omega = \Omega(\varphi_x)$ for the elastic-waves of the Po leads, in the first Brillouin zone is given in Fig.2. $\Omega^2 = \frac{\omega^2}{\omega_0^2}$ a dimensionless frequency, normalized with respect ω_0 characteristic lattice frequency The dispersion branches of the spin-wave modes localized on the bcc Ni nanostructure forthe system - Fe[Ni(*n*)]Fe – are calculated using Eq.(7).

In Fig.3a are presented the computed results of the dispersion branches of the elatic-wave modes localized on the cfc Cu nanostructure .These localized elastic-wave modes propagate along the y direction parallel to the lamellar Ni layers, but are localized along the x direction on both sides of the nanostructure. The shaded areas denote the elastic-wave bands of the Po leads projected along the y axis.There are three branches of localized spin wave modes, ofwhich two are at low energies [~0.25 to 2 meV], and the third is at the relatively higher energies [~5to 6.3meV]. A fourth branch at high energies[~ 8 to 14meV] is a resonance eigenmodeentirely inside the Fe spin-waves continuum. The spin precession displacements of the *two low energy modes* are associated to the spin dynamics on theNi sites of the *two monatomic layers*of thecorresponding bcc Ni nanostructure, whereas the third, relatively higher energy, is associated to the spin dynamics on the Fe and Ni interfacial sites, but primarily the interfacial Fe sites.The resonance branch at clearly high energies is uniquely a resonance mode on the Fe sites of the leads.The two low energy branches at[~0.5 to 2 meV], carried by the Ni sites are reminiscent of the acoustic and optic branches for the vibrational modes of a binary atomic chain, the difference being that the two Ni spins are identical and the two curves are degenerate at the upper limit of their BZ; both extend as resonances inside the Fe spin-wave continuum. The third branch of localized modes at energies [~5to 6.3meV], is an optic mode carried by the adjacent interfacial Ni and Fe sites, is clearly separate from the two others at the lower energies; it also extends for the larger part of its wave-vector zone mostly into the Fe bands continuum.

In Fig.3b are presented the computed results of the dispersion branches of the spin-wave modes localized on the bcc Ni nanostructure of fourbcc Ni monatomic layers between the bcc Fe leads forthe system - Fe[Ni(4)]Fe -. The outlay is similar to that of Fig.3a.There are five branches of localized spin wave modes, of which four are at low energies [~0.3 to 3meV], and the fifth is at the relatively higher energies [~5to 6.3 meV]; note, however, that the two small separate parts of its branch at the centre of the wave-vector zone, observed for the - Fe[Ni(2)]Fe -system, coalesce to become one for the - Fe[Ni(4)]Fe - system. The spin precession displacements of the *four low energy modes* are associated to the spin dynamics on the Ni sites of the *four monatomic layers* of the corresponding bcc Ni nanostructure.The resonance branch at high energies [~ 8 to 14meV] rest unchanged.

In Fig.3c are presented the computed results of the dispersion branches of the spin-wave modes localized on the bcc Ni nanostructure of fivebcc Ni monatomic layers between the bcc Fe leads forthe system - Fe[Ni(5)]Fe -. The outlay is similar to that of Fig.3a and Fig.3b.There are six branches of localized spin wave modes, of which five are at low energies [~0.3 to 3meV], and the fifth is at the relatively higher energies [~5to 6.3 meV]; note, however, that the two small separate parts of its branch at the centre of the wave-vector zone, observed for the - Fe[Ni(2)]Fe - system, coalesce to become one for the - Fe[Ni(4)]Fe - system. The spin precession displacements of the *five low energy modes* are associated to the spin dynamics on the Ni sites of the *five monatomic layers* of the corresponding bcc Ni nanostructure.The resonance branch at high energies [~ 8 to 14meV] rest unchanged.

The analysis of the results in Figs.3 imply that the two localized spin-wave modes at the higher energies, namely at [~5to 6.3 meV], and at [~ 8 to 14meV], are both primarily resonance modes in the Fe spin-wave continuum, and rest unchanged when increasing the thickness of the bcc Ni nanostructure by adding additional Ni monatomic layers. Further, the localized spin-wave modes at low energies [~0.3 to 3meV] correspond to modes which are excited by virtue of the spin precession displacements on uniquely the sites of the Ni nanostructure. The number of these low energy modes mirrors the number of the bcc Ni monatomic layers of the Ni nanostructure. The two high energy resonances, carried by Fe sites, and inside the Fe spin-wave continuum, seemingly compress the low energy modes, carried on Ni sites, to within a limited interval of energy. The multiplication of bcc Ni monatomic layers generates well defined localized spin-wave modes inside this interval.

In Fig.4 we illustrate the behavior of the local density of states (LDOS) for the localized spin-wave modes, including localized states and resonances, for the systems under study, by

presenting the computed LDOS results for the - Fe[Ni(4)]Fe - system. Since the bcc Ni nanostructure of *n* Ni monatomic layers and two adjacent Fe monatomic layers of the leads, constitute together a symmetric ensemble, (see Fig.1 for reference), we expect that the LDOS for corresponding symmetric sites be identical. This is indeed the case. There are three LDOS individual figures in arbitrary units, as functions of the normalized frequency Ω: the first for the (Ni:1,2)boundary sites,the second for (Ni:3,4), and the third for (Fe:5,6). By comparing Fig.3b with Fig.4 it is clear how the different LDOS on the nanostructure boundary sites correspond to the localized spin-wave modes.

The ballistic coherent reflection and transmission scattering coefficients, r and t, for incident spin-waves from the Fe leads, across the lamellar bcc Ni nanostructure in the - Fe[Ni(n)]Fe - systems, are calculated using Eq.(9). The ballistic coherent reflection and transmission scattering cross sections, $R$and T,are calculated using Eqs.(10).

In Fig.5a are presented the computed results for the magnonicballistic coherent reflection and transmission scattering cross sections, respectively$R$ (continuous curve) and T (dashed curve), for spin-waves of the Fe leads incident at normal incidence across the embedded lamellar bcc Ni nanostructure of two monatomic layers between the Fe leads, in the system - Fe[Ni(2)]Fe –.The scattering cross sections R and T are computed as functions of the normalized frequency $\Omega = \hbar\omega\,/J_{Fe-Fe}S_{Fe}$. The two spectral peaks of the ballistic transmission spectra are well defined at ≈ 0.25 meV and ≈ 2 meV; they correspond to Fabry-Perot spectral resonances due to the interaction of incident Fe spin-waves with the low energy localized spin-wave resonance modes in Fig.3a. This Fabry-Perot spectral resonance phenomenon is also evident in the computed results presented in Fig.5b and Fig.5c for the ballistic coherent transmission spectra; in these figures the respective four and five well defined spectral peaks of the transmission spectra, for the - Fe[Ni(4)]Fe - and - Fe[Ni(5)]Fe - systems, correspond in each case to the interaction of incident Fe spin-waves with the low energy localized spin-wave resonance modes in Fig.3a and Fig.3b. As discussed earlier these low energy modes are carried by the Ni sites on the Ni nanostructure.

In conclusion, we have developed a theoretical model for the magnonic ballistic coherent transport across ultrathin ferromagnetic lamellar bcc Ni nanostructures between Fe leads, in thermodynamically stable systems. The spin-wave localized eigenmodes, notably the resonanceeigenmodes, confinedstrictly to the bcc Ni ultrathin nanostructures in these systems,just as a quantum well, give rise to interactions with the incident Fe lead spin-waves that generate highly refined Fabry-Perot resonances at specific energies in the ballistic coherent transmission spectra. Theballistic coherent transmission properties of these lamellar Fe-Ni systems may be of technological use, to controlthe transmission of specific magnonicfrequencies, and conversely the suppression of magnonic signals in magnonic and spintronic nano-devices.

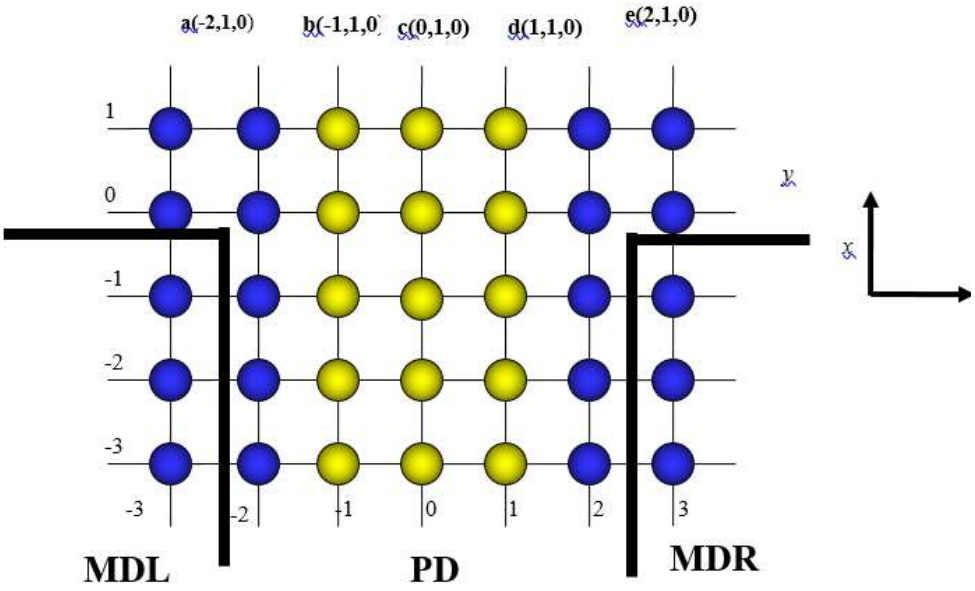

Figure 1. *The system model of the plan defect of the Cu integrated in simple cubic Po crystal.*

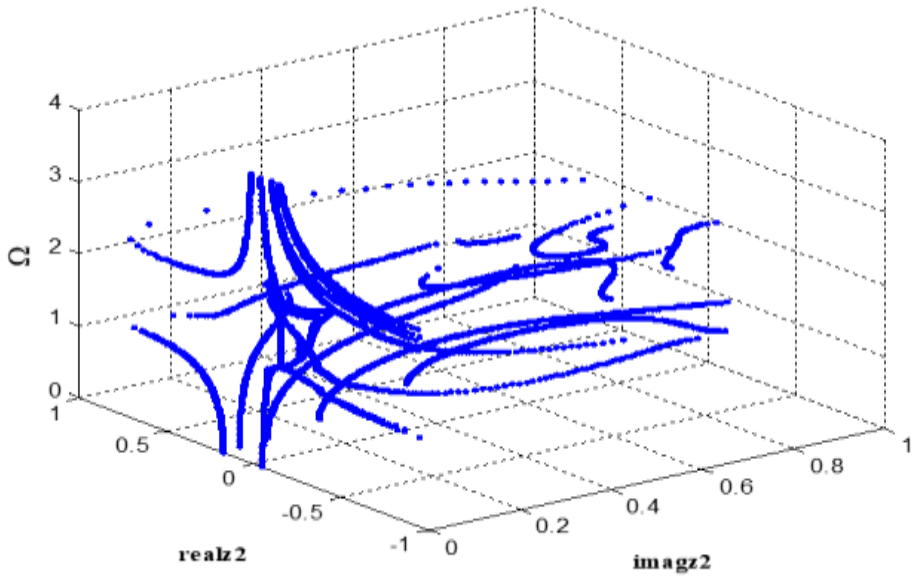

Figure 2. *Representation 3D of the evanescent phase factors η_2 in the b*

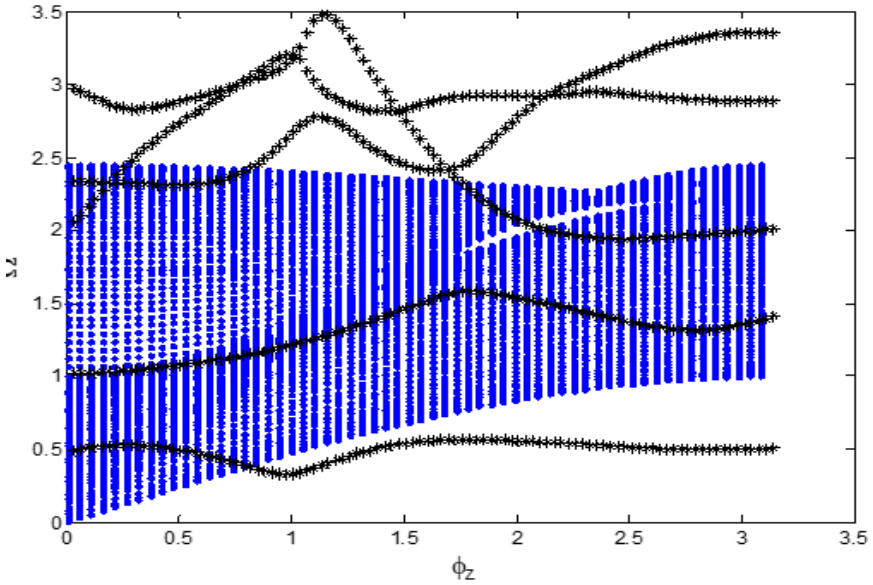

Figure 3. *The localized Rayleigh dispersion branches for φ_z running over [0, 3.5], $r_0 = 0.25$, e'= 0.3, r1= 0.76 r2 = 0.12, $r_4 = 0.063$ and $r_3 = 0.63$.*

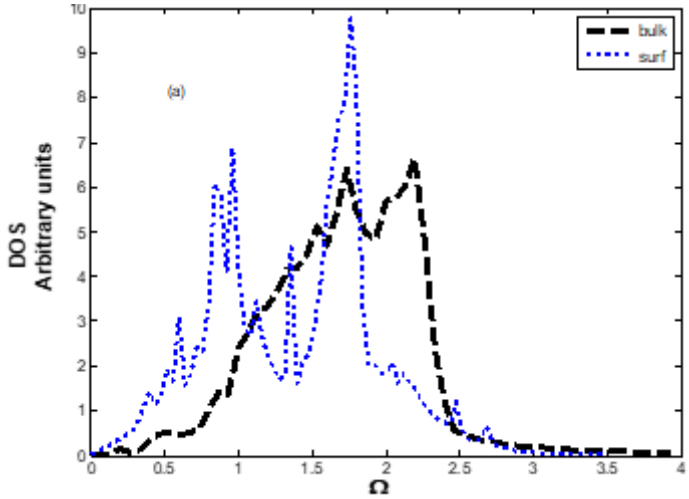

Figure 4a *The vibrational state densities (DOS) of respectively of the site*

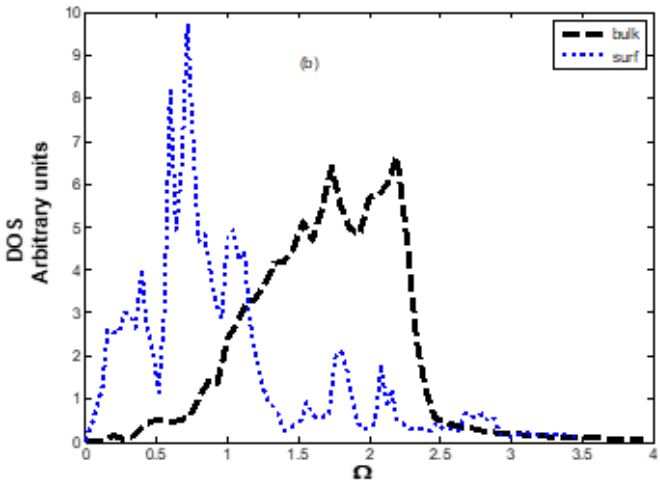

*Figure 4 (**b**) as function of dimensionless frequency* Ω *and the system parameters* r_0 *= 0.25, e'= 0.3,* r_1*= 0.76, r2 = 0.12,* r_4 *= 0.063 and* r_3 *= 0.63.*

Author Statements:

- **Ethical approval:** The conducted research is not related to either human or animal use.
- **Conflict of interest:** The authors declare that they have no known competing financial interests or personal relationships that could have appeared to influence the work reported in this paper
- **Acknowledgement:** The authors declare that they have nobody or no-company to acknowledge.
- **Author contributions:** The authors declare that they have equal right on this paper.
- **Funding information:** The authors declare that there is no funding to be acknowledged.
- **Data availability statement:** The data that support the findings of this study are available on request from the corresponding author. The data are not publicly available due to privacy or ethical restrictions.
- **Use of AI Tools:** The author(s) declare that no generative AI or AI-assisted technologies were used in the writing process of this manuscript.

References

1. A.A.Maradudin, R.F.Wallis, *L.Dobrzynski*, *Handbook of surface and interface* vol.3 ,(Garland, New York) , 1980.
2. rmand .G, Masri. P, *Surf. Sci.* **130,** 89 (1989).
3. H. Ibach, J.Vac.Sci. *Technol.A* ***55,*** 440 (1987).
4. H. Ibach D.L, Mills (eds), *Electron Energy Loss Spectroscopies and surfaces vibrations (New Academic York*), 1982.
5. See for are wiew article, G.Bendek and J.P.Toennies, *Surf.Sci. 299/300***,** .587 (1994).
6. A.A Maradudin, E.W.Montrol, GH.Weiss and I.P. Ipatova, *theory of Lattice Dynamics in the Harmoni approximation. edited by Academic New York,1971*
7. A.A. Maradudin, R.F.Wallis and L.Dobbrzynski, *Handbook of Surfaces and Interfaces, Vol.3 (Garland, New York), 1980.*
8. L.Dobrzynski and D.Millis, J.Phys.Chem.Solids 30**,** 1043.(1969)
9. R.E. Allen, G.P. Alldredge and F.W. de Wette, *Phys.Rev* 4-**6,** 1682 (1971).
10. T.E. Feuchtwang, *Phys.Rev.****155,*** 715 **(**1967).
11. J.Szeftel, A. Khater, *J. Phys. C: Solid State Phys.* ***20,*** 4725 (1988).
12. A. Khater, N. Aubay , D. Kechrakos, *J. Phys: Condens. Matter 4***,** 7343 **(**1992).
13. Black J. E , Bopp. P, *Surf .Sci 140*, 275 (1984)
14. Knipp P, *Phys. Rev. B 43,* 6908 (1991).
15. G.Brusdeylin, R.B.Doak, J.P Tonnies, *Phys.Rew.B* 27, 3662 (1983)
16. Mele E. J , Pykhtin M. V, *Phys. Rev.Lett.* ***75,*** 3878 **(**1995).
17. A.Fellay, F .Gagel, K.Maschke, A.Virlouvet, A.Khater, *Phys. Rev.B* ***55,*** 1707 **(**1999).
18. A.Virlouvet, A.Khater, H.Aouchiche, O.Rafil, K.Maschke, *Phys. Rev. B 59***,** 4933. (1999).
19. A. Khater, W.Czaja, *Physica B* ***167,*** 33 **(**1990).
20. A.Tekman, P.F Bagstep, *Phys.Rev.B* ***48***, 2553 (1993).
21. B.Shapiro, *Phys. Lett.* ***65,*** 1510 (1990) .
22. B.Stefano de Gironcoli, Stefano Baroni, *Phys.Lett.* ***63,*** 1959 (1992).
23. Y.Pennec, A. Khater, *Surf. Sci. Lit.* ***348,*** 82 (1996).
24. A.A Maradudin, E.W.Montroll and G.H. Weiss, *Theory of Lattice Dynamics in the Harmonic Approximation, Solid State Physics: Advances in Research and Application, suppl.3, Academic Press,New York& London*, 1963
25. H.Grimech, A.Khater, *Surf.Sci.* ***323,*** 198(1995).
26. M.Belhadi, O.Rafil, R.Tigrine, A.Khater, J.Hary, A.Virlouvet, K.Maschke, *Eur.Phys. J. B* .***15,*** 435 **(**2000),
27. M.Belhadi, A.Khater, O.Rafil, J.Hardy, R.Tigrine, *Phys.Stat.solidi.(b)*,228, 685(2001).

28. D.Marcuse in *Quantic Electronics, principles and application edited by P.F Liao and P.L Kelly ,Academic press ,New York, 1991*.
29. B. Bourahla, A. Khater, R. Tigrine *Eur. Phys. J. B 69*, 343 (2009)
30. R.Tigrine *A. Khater R. , B. Bourahla Eur.phys.J.B62*, 59 (2008).
31. Khater, R. Tigrine and B. Bourahla, *Physica status Solidi b,vol 246 ,Issue 7*, 1614 (2009) .
32. A.A Maradudin, E.W.Montroll, G.H. Weiss and I.P. Ipatova, *Theory of Lattice Dynamics in the Harmonic Approximation, edited by Academic New York, 1971.*
33. S. Amoudache, R. Tigrine, A. Khater and B. Bourahla**,** Eur. Phys. J. B **73**, 405 (2010) .
34. A.F. Devonshire, Proc.R.Soc.London**,** Ser.A 158, 269 (1937) .
35. C.Stranchan, *Proc.R.Soc.London Ser.A **158***, 591 (1937)
36. F.O Goodman, CRC Crit. Rev. Solid State Mater.Sci.**7**, 33 (1977).
37. J.P. Toennies, in *Dynamics of Gas Surface Interactions Vol.**21** of Spring Series in Chemical Physics,2, edited by G.Benedek and U.Valbusa(Springer, Berlin,198,* 208 *(1982).*